The Abdus Salam
International Centre for Theoretical Physics

United Nations
Educational, Scientific and
Cultural Organization

IAEA
International Atomic Energy Agency

1960-10

ICTP Conference Graphene Week 2008

25 - 29 August 2008

Electronic propertiesofcorrugatedgraphene

Authors:

A. Castro-Neto *(Boston U.),* **N. M. R. Peres** *(U. Minho, Portugal),* **E. V. Castro, J. dos Santos** *(Porto),* **J. Nilsson** *(Boston U.),* **A. Morpurgo** *(Delft),* **M. I. Katsnelson** *(Nijmegen),* **D. Huertas-Hernando** *(Trondheim, Norway),* **D. P. Arovas, M. M. Fogler** *(U. C. San Diego),* **J. González, F. G., M. P. López-Sancho, T. Stauber, J. A. Vergés, M. A. H. Vozmediano, B Wunsch** *(CSIC, Madrid),* **A. K. Geim, K. S. Novoselov** *(U. Manchester),* **A. Lanzara** *(U. C. Berkeley),* **M. Hentschel** *(Dresden),* **E. Prada, P. San-José** *(Karlsruhe),* **J. L. Mañes** *(U. País Vasco, Spain),* **F. Sols** *(U. Complutense, Madrid),* **E. Louis** *(U. Alicante, Spain),* **A. L. Vázquez de Parga, R. Miranda** *(U. Autónoma, Madrid),* **B. Horowitz** *(Beersheva),* **P. Le Doussal** *(ENS, Paris)*

Electronic properties of corrugated graphene.

A. Castro-Neto (Boston U.)
N. M. R. Peres (U. Minho, Portugal)
E. V. Castro, J. dos Santos (Porto), J. Nilsson (Boston U.), A. Morpurgo (Delft), M. I. Katsnelson (Nijmegen), D. Huertas-Hernando (Trondheim, Norway), D. P. Arovas, M. M. Fogler (U. C. San Diego), J. González, F. G., M. P. López-Sancho, T. Stauber, J. A. Vergés, M. A. H. Vozmediano, B Wunsch (CSIC, Madrid), A. K. Geim, K. S. Novoselov (U. Manchester), A. Lanzara (U. C. Berkeley), M. Hentschel (Dresden), E. Prada, P. San-José (Karlsruhe), J. L. Mañes (U. País Vasco, Spain), F. Sols (U. Complutense, Madrid), E. Louis (U. Alicante, Spain), A. L. Vázquez de Parga, R. Miranda (U. Autónoma, Madrid), B. Horowitz (Beersheva), P. Le Doussal (ENS, Paris).

Outline

- Disorder and the Dirac equation
- Lattice strains, topological defects and curvature
- Effective magnetic fields
- Random gauge fields
- Zero modes, interaction effects
- Strains in suspended samples

Midgap states and charge instabilities in corrugated graphene, F. G., M. I. Katsnelson, and M. A. H. Vozmediano, Phys. Rev. B 77, 075422 (2008)
Gauge field induced by ripples in graphene, F. G., B. Horowitz and P. Le Doussal, Phys. Rev. B 77, 205421 (2008)
Pseudomagnetic fields and ballistic transport in suspended graphene sheets, M. M. Fogler, F. G., and M. I. Katsnelson, ArXiv:0807.3175
The electronic properties of graphene, A. H. Castro Neto, F. G., N. M. R. Peres,..A. K. Geim, K. S. Novoselov, ArXiv:0709.1163, Rev. Mod. Phys., in press

Effective gauge fields

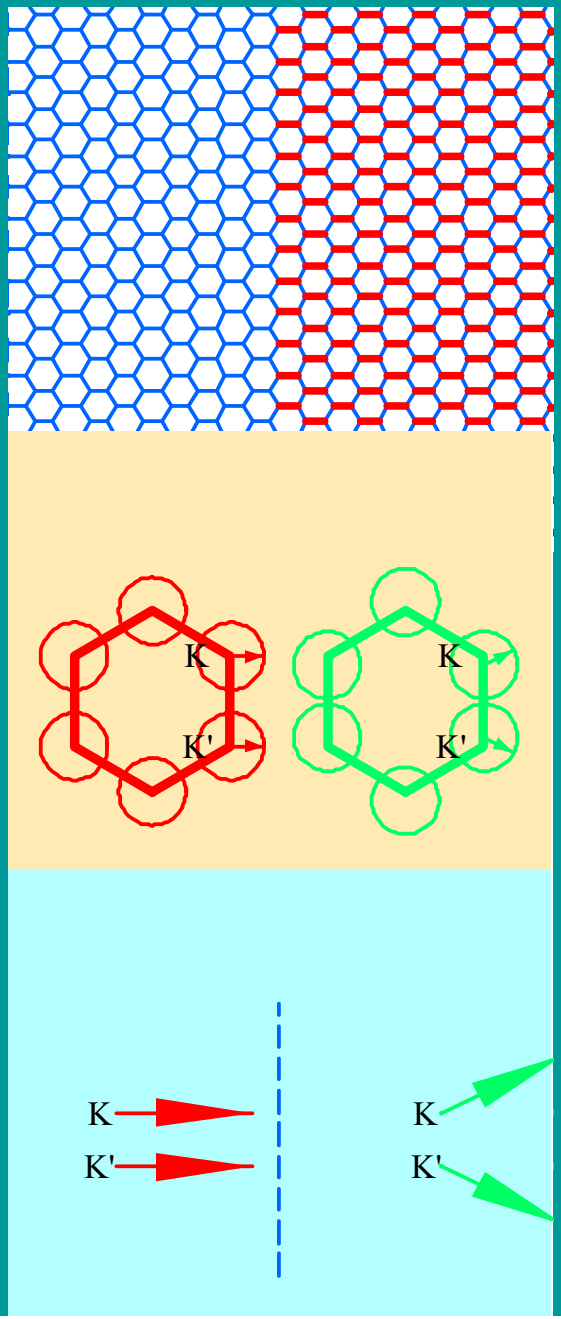

$$H \equiv \begin{pmatrix} 0 & t_1 e^{i\vec{k}_1\vec{a}_1} + t_2 e^{i\vec{k}_2\vec{a}_2} + t_3 e^{i\vec{k}_3\vec{a}_3} \\ t_1 e^{-i\vec{k}_1\vec{a}_1} + t_2 e^{-i\vec{k}_2\vec{a}_2} + t_3 e^{-i\vec{k}_3\vec{a}_3} & 0 \end{pmatrix} \approx \begin{pmatrix} 0 & \frac{3\bar{t}a}{2}\left(k_x + ik_y\right) + \Delta t \\ \frac{3\bar{t}a}{2}\left(k_x + ik_y\right) + \Delta t & 0 \end{pmatrix}$$

A modulation of the hoppings leads to a term which modifies the momentum: an effective gauge field.

The induced “magnetic” fields have opposite sign at the two corners of the Brillouin Zone.

These terms are forbidden by symmetry in clean graphene.

Suspended graphene. Graphene membranes

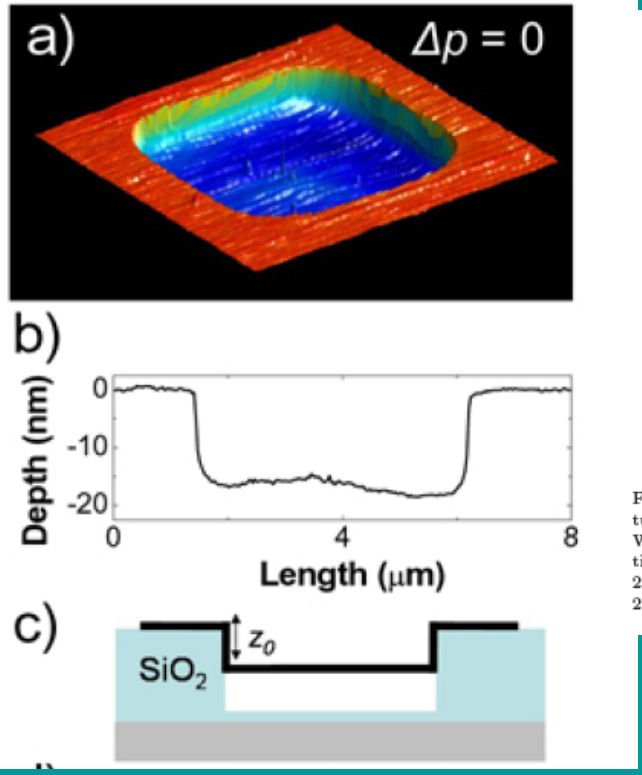

J. S. Bunch, S. S. Verbridge, J. S. Alden, A. M. van der Zande, J. M. Parpia, H. G. Craighead, and P. L. McEuen, ArXiv:0805.3309

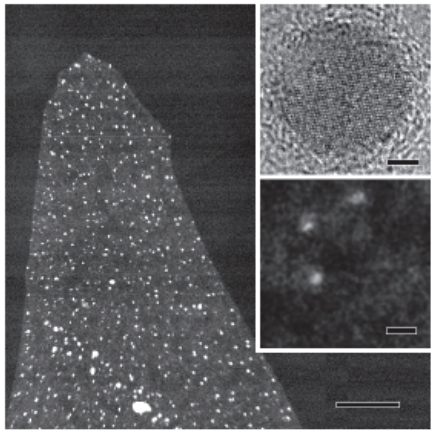

Figure 4: HAADF micrograph of a section of a graphene membrane tl tured during annealing. The graphene crystal is supported from one si White dots are copper nanoparticles. Scale bar: 1μm. Top inset: higl tion bright field STEM micrograph of such a Cu particle (⌀ 8.0 nm; s 2 nm). Low inset: HAADF image of individual atoms on graphene; s 2 Å.

T. J. Booth, P. Blake, R. R. Nair, D. Jiang, E. W. Hill, U. Bangert, A. Bleloch, M. Gass, K. S. Novoselov, M. I. Ktasnelson, and A. K. Geim, ArXiv:0805.188

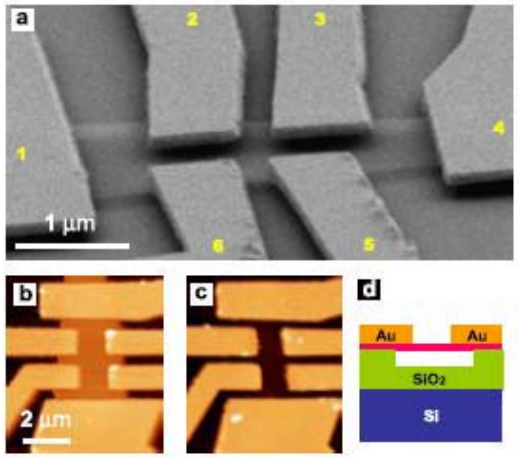

FIG. 1: (a) SEM image of a typical suspended six-probe graphene device taken at 15° with respect to the sample plane. (b) AFM image of the suspended device #1 before the measurements. (c) AFM image of the device #1 after the measurements with graphene removed by a short oxygen plasma etch (same z scale). (d) Device schematic, side-view. Degenerately doped silicon gate (blue), partly etched SiO_2 (green), suspended single-layer graphene (pink) and Au/Cr electrodes (orange).

K. I. Bolotin, K. J. Sikes, Z. Jiang, G. Fudenberg, J. Hone, P. Kim, and H. L. Stormer, ArXiv:0802.2389

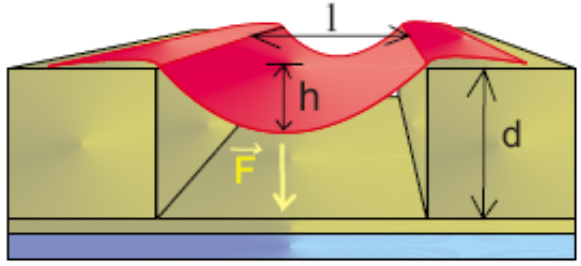

M. M. Fogler, F. G., M. I. Katsnelson, ArXiv:0807.3175

Lattice frustration as a gauge potential.

J. González, F. G. and M. A. H. Vozmediano, Phys. Rev. Lett. **69**, 172 (1992)

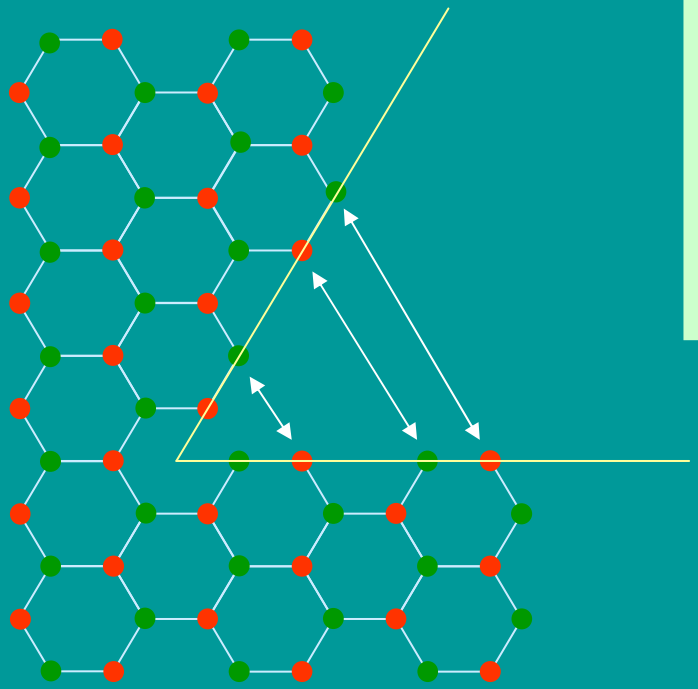

- **A fivefold ring defines a disclination.**
- **The sublattices are interchanged.**
- **The Fermi points are also interchanged.**
- **These transformations can be achieved by means of a gauge potential.**

$$i\vec{\nabla} \rightarrow i\vec{\nabla} - \vec{A}\begin{pmatrix} 0 & 1 \\ 1 & 0 \end{pmatrix}$$

$$\Phi = \int \vec{A}\, d\vec{l}$$

The flux Φ is determined by the total rotation induced by the defect.

Continuum model of the fullerenes.

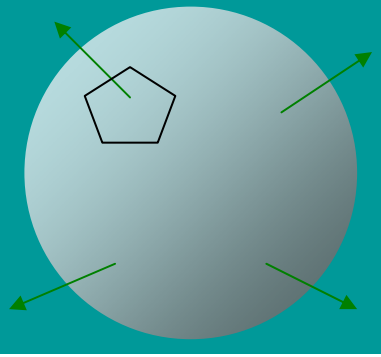

- Dirac equation on a spherical surface.
- Constant magnetic field (Dirac monopole).

$$\frac{\hbar v_F}{R}\left[i\partial_\theta - \frac{1}{sin(\theta)}\partial_\phi + \frac{i(1+l)cos(\theta)}{2\,sin(\theta)}\right]\Psi_a = \varepsilon\Psi_b$$

$$\frac{\hbar v_F}{R}\left[i\partial_\theta + \frac{1}{sin(\theta)}\partial_\phi + \frac{i(1-l)cos(\theta)}{2\,sin(\theta)}\right]\Psi_b = \varepsilon\Psi_a$$

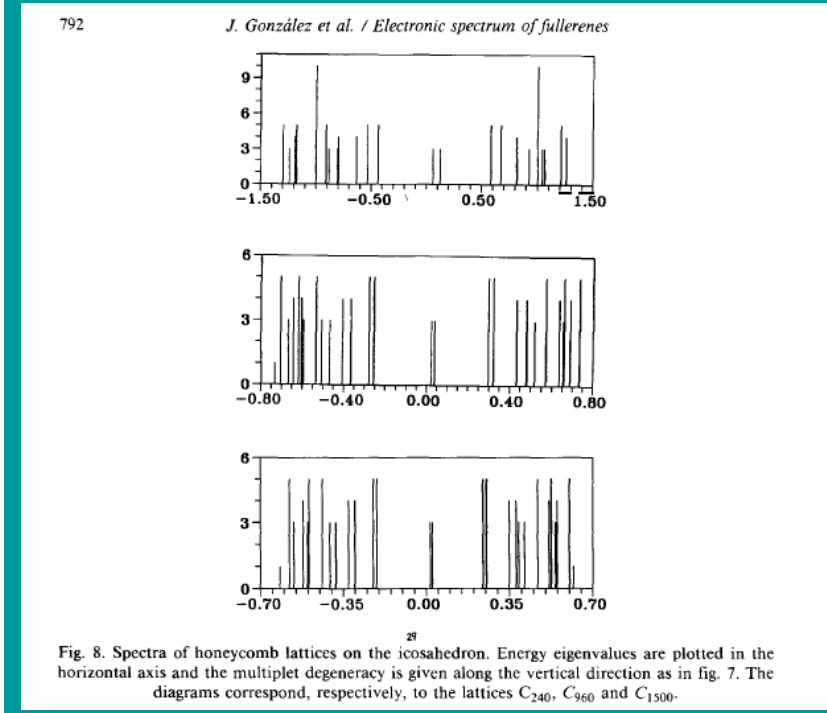

792 J. González et al. / Electronic spectrum of fullerenes

Fig. 8. Spectra of honeycomb lattices on the icosahedron. Energy eigenvalues are plotted in the horizontal axis and the multiplet degeneracy is given along the vertical direction as in fig. 7. The diagrams correspond, respectively, to the lattices C_{240}, C_{960} and C_{1500}.

$$\varepsilon_J = \frac{\hbar v_F}{R}\sqrt{\left[J(J+1)\right] - l(l+1)} \qquad J \geq l$$

J. González, F. G., and M. A. H. Vozmediano,
Nucl. Phys.B 406, 771 (1993)

Effective gauge fields
In plane elastic deformations

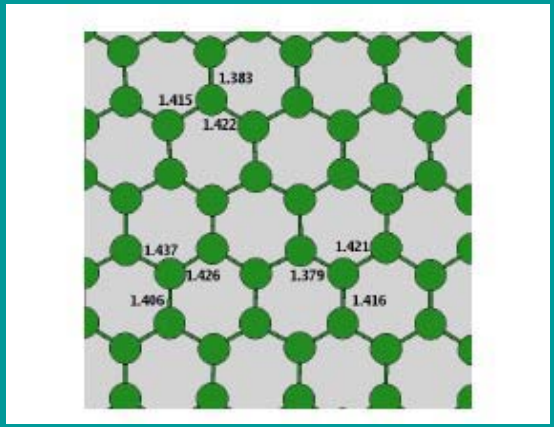

H. Suzuura and T. Ando, Phys. Rev. B **65**, 235412 (2002)
J. L. Mañes, Phys. Rev. B **76**, 045430 (2007)

$$H \equiv \begin{pmatrix} 0 & v_F\left(k_x + ik_y\right) + \beta t\left(u_{xx} - u_{yy} - 2iu_{xy}\right) \\ v_F\left(k_x - ik_y\right) + \beta t\left(u_{xx} - u_{yy} + 2iu_{xy}\right) & 0 \end{pmatrix}$$

$$\beta = \frac{\partial \log(t)}{\partial \log(a)} \approx 2$$

A. Fasolino, J. H. Los, and M. I. Katsnelson, Nature Mat. **6**, 858 (2007)

Elastic strains imply deformations of bonds, and modulations of hoppings.

$$\frac{\partial^2 u_{ij}}{\partial x_k \partial x_l} + \frac{\partial^2 u_{kl}}{\partial x_i \partial x_j} - \frac{\partial^2 u_{il}}{\partial x_j \partial x_k} - \frac{\partial^2 u_{jk}}{\partial x_i \partial x_l} = 0$$

$$R_{ijkl} = \frac{1}{2}\left(\frac{\partial^2 g_{ij}}{\partial x_k \partial x_l} + \frac{\partial^2 g_{kl}}{\partial x_i \partial x_j} - \frac{\partial^2 g_{il}}{\partial x_j \partial x_k} - \frac{\partial^2 g_{jk}}{\partial x_i \partial x_l}\right) + O\left(g^2\right)$$

Saint Venant's compatibility conditions imply zero intrinsic curvature

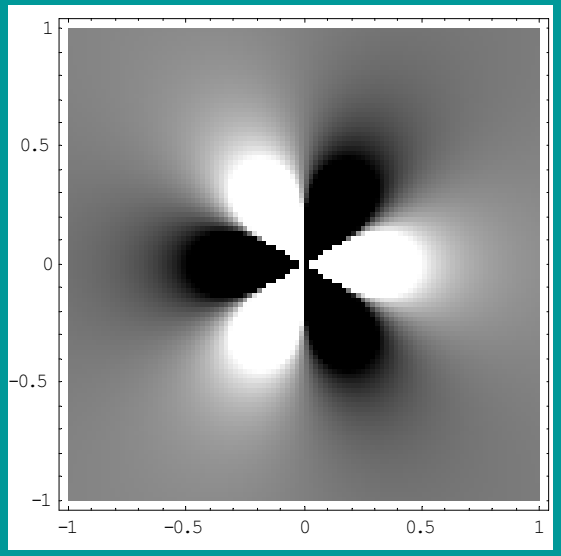

Effective magnetic field induced around a dislocation.

The gauge field associated to elastic strains is material dependent, and it does not imply intrinsic curvature.

Effective gauge fields

Misalignment of π orbitals

A. H. Castro Neto and E.-A. Kim, arXiv:cond-mat/0702562

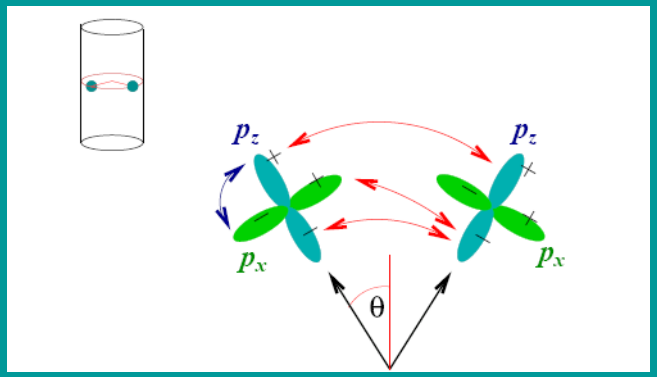

A finite curvature induces the mixing of π and σ orbitals, and modifies the effective hoppings.

$$\delta t \approx \left(-\frac{1}{3} t_{pp\pi} + \frac{1}{2} t_{pp\sigma} \right) \left[(\vec{a}\nabla)\nabla h \right]^2$$

$$A_x \propto \left(\frac{\partial^2 h}{\partial x^2} \right)^2 - \left(\frac{\partial^2 h}{\partial y^2} \right)^2$$

$$A_y \propto -2 \frac{\partial^2 h}{\partial x \partial y} \left(\frac{\partial^2 h}{\partial x^2} + \frac{\partial^2 h}{\partial y^2} \right)$$

The gauge field associated to the misalignment of π orbitals is material dependent, and it does not imply intrinsic curvature.

Non abelian gauge potential II.

$$
\begin{array}{c|cccc}
 & |KA\rangle & |KB\rangle & |K'A\rangle & |K'B\rangle \\
|KA\rangle & 0 & v_F\left(k_x - ik_y\right) & v_F\left[-iA_x(\vec{r}) - A_y(\vec{r})\right] & 0 \\
|KB\rangle & v_F\left(k_x + ik_y\right) & 0 & 0 & v_F\left[iA_x(\vec{r}) - A_y(\vec{r})\right] \\
|K'A\rangle & v_F\left[iA_x(\vec{r}) - A_y(\vec{r})\right] & 0 & 0 & v_F\left(k_x + ik_y\right) \\
|K'B\rangle & 0 & v_F\left[-iA_x(\vec{r}) - A_y(\vec{r})\right] & v_F\left(k_x - ik_y\right) & 0
\end{array}
$$

Dirac hamiltonian for the two valleys, with Umklapp scattering.

$$
\begin{array}{c|cccc}
 & |KA\rangle + i|K'B\rangle & |KB\rangle - i|K'A\rangle & |KA\rangle - i|K'B\rangle & |KB\rangle + i|K'A\rangle \\
|KA\rangle + i|K'B\rangle & 0 & v_F\left(k_x + A_x - ik_y - iA_y\right) & 0 & 0 \\
|KB\rangle - i|K'A\rangle & v_F\left(k_x + A_x + ik_y + iA_y\right) & 0 & 0 & 0 \\
|KA\rangle - i|K'B\rangle & 0 & 0 & 0 & v_F\left(k_x - A_x + ik_y - iA_y\right) \\
|KB\rangle + i|K'A\rangle & 0 & 0 & v_F\left(k_x - A_x - ik_y + iA_y\right) & 0
\end{array}
$$

Intervalley scattering acts as a gauge potential which rotates the valley index.
It plays a similar role to the potential induced by pentagons and heptagons.

Gauge potentials

Physical origin

Elastic strains
Mixing of σ and π bands (extrinsic curvature)
Topological defects (intrinsic curvature)

Effects

Elastic strains
Intravalley scattering
Intervalley scattering (non commuting gauge fields)

Effective gauge fields

Effective magnetic length:

$$l_B \propto \begin{cases} l\left(\frac{l}{h}\right) \\ l\sqrt{\frac{t}{E}\frac{l^3}{ah^2}} \\ l\sqrt{\left(\frac{\partial \log(t)}{\partial \log(a)}\right)^{-1}\frac{al}{h^2}} \end{cases}$$

Intrinsic curvature

Mixing between π and σ orbitals

Elastic strains

Some estimates: h=1nm, l=10nm, a=0.1nm

$$l_B \approx \begin{cases} 100nm & B \approx 0.06T \\ 1000nm & B \approx 0.0006T \\ 10nm & B \approx 6T \end{cases}$$

Intrinsic curvature

Mixing between π and σ orbitals

Elastic strains

Ripples in graphene

J. C. Meyer, A. K. Geim, M. I. Katsnelson, K. S. Novoselov, T. J. Booth and S. Roth, Nature **446**, 60 (2007).
J. C. Meyer, A. K. Geim, M. I. Katsnelson, K. S. Novoselov, D. Obergfell, S. Roth, C. Girit and A. Zettl, Sol. St. Commun. **143**, 101 (2007).

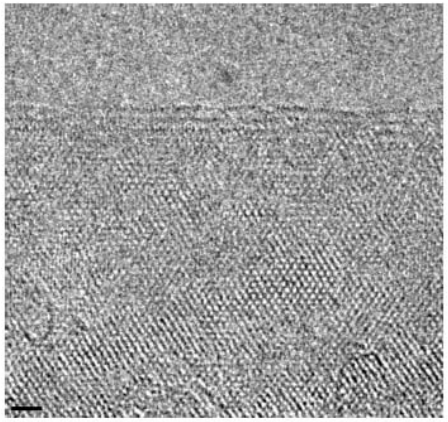

Figure 4 | Atomic resolution imaging of graphene membranes. TEM image of a few-layer graphene membrane near its edge, where the number of dark lines indicates the thickness of two to four layers. Because for few-layer graphene the electron contrast depends strongly on incidence angle, relatively small (a few degrees) variations in the surface normal become visible. The atomic-resolution imaging was achieved by using FEI Titan at an acceleration voltage of 300 kV. Scale bar, 1 nm.

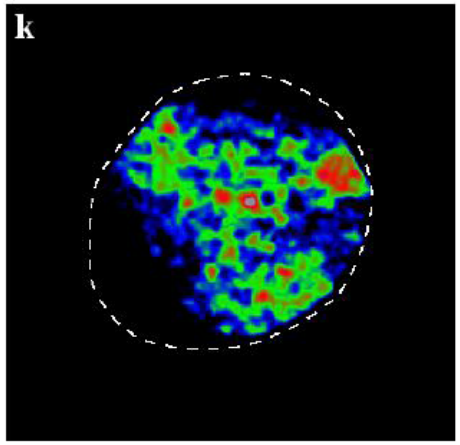

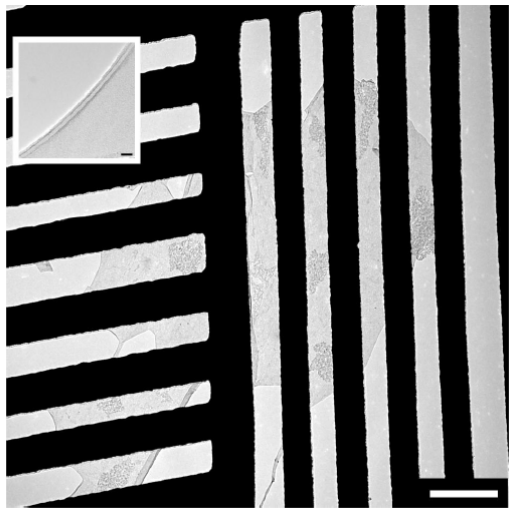

Figure 1: TEM image of suspended graphene (darker gray areas) supported by a microfabricated metal grid (black lines). The inset shows a scroll at the edge. Scale bar 1 μm, and 20 nm for the inset.

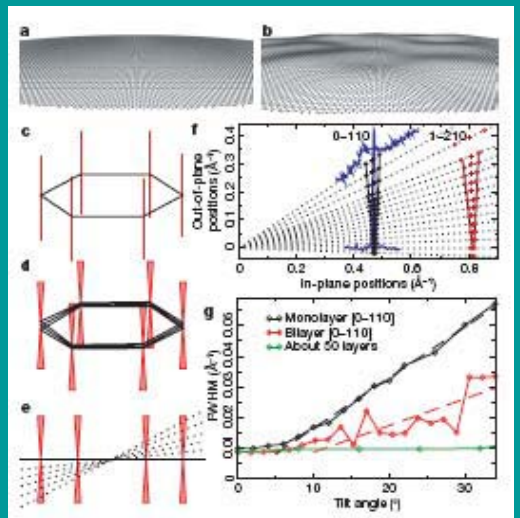

Figure 3 | Microscopically corrugated graphene. **a**, Flat graphene crystal in real space (perspective view). **b**, The same for corrugated graphene. The roughness shown imitates quantitatively the roughness found experimentally. **c**, The reciprocal space for a flat sheet is a set of rods (red) directed perpendicular to the reciprocal lattice of graphene (black hexagon). **d**, **e**, For the corrugated sheet, a superposition of the diffracting beams from microscopic flat areas effectively turns the rods into cone-shaped volumes so that diffraction spots become blurred at large angles (indicated by the dotted lines in **e**) and the effect is more pronounced further away from the tilt axis (compare with Fig. 2). Diffraction patterns obtained at different tilt angles allow us to measure graphene roughness. **f**, Evolution of diffraction peaks with tilt angle in monolayer graphene. The experimental data are presented in such a way that they closely resemble the schematic view in **e**. For each tilt angle, the black dotted line represents a cross-section for diffraction peaks (0–110) and (1–210). The peak centres and full widths at half maxima (FWHM) in reciprocal space are marked by crosses and open circles, respectively. In two cases (0° and 34°), the recorded intensities are shown in full by blue curves. All the intensity curves could be well fitted by the gaussian shape. The solid black lines show that the width of the diffraction spots reproduces the conical broadening suggested by our model (**d** and **e**). **g**, FWHM for the (0–110) diffraction peak in monolayer and bilayer membranes and thin graphite (as a reference), as a function of tilt angle. The dashed lines are the linear fits yielding the average roughness. The flat region between 0° to 5°, and also for the reference sample, is due to the intrinsic peak width for the microscope at our settings.

Ripples in graphene

Single layer graphene on SiO_2

M. Ishigami, J. H. Chen, W. G. Cullen, M. S. Fuhrer and E. D. Williams, Nano Letters **7**, 6 (2007)
E. Stolyarova, K. T. Rim, S. Ryu, J. Maultzsch, P. Kim, L. E. Brus, T. F. Heinz, M. S. Hybertsen and G. W. Flynn, Proc. Nat. Acad. Sci. **104**, 9209 (2007)

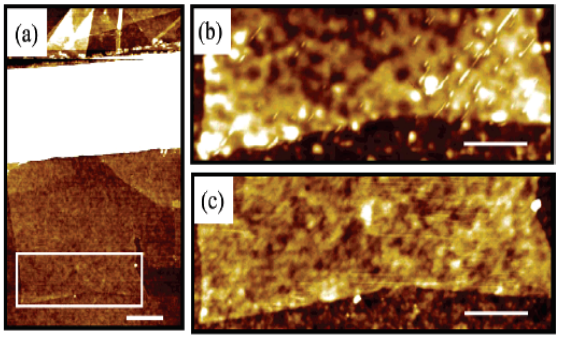

Figure 2. (a) AFM topography of graphene deposited on SiO_2. Thin graphite flakes are generated using the mechanical exfoliation technique[1] on thermally grown SiO_2 with the thickness of 300 nm. Monolayer graphite flakes (graphene) are located using optical and atomic force microscopy.[8] The e-beam lithography defined electrode,[33] approximately 80 nm in height and 1.5 μm in width, is the white area nearly horizontal to the image. The black square indicates the region shown in parts b and c of Figure 1. The scale bar is 500 nm. (b) Graphene sheet prior to the cleaning procedure described in text. The scale bar is 300 nm. (c) Graphene sheet after the cleaning procedure. The standard deviation of the height variation in a square of side 600 nm is approximately 3 Å after the treatment compared to 8 Å before the treatment. The scale bar is 300 nm. Images a–c were acquired using intermittent-contact mode AFM in air.

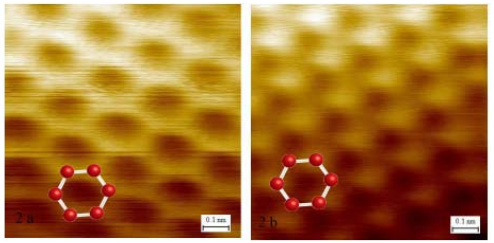

Figure 2. STM topographic images of different regions of the graphene flake of Fig. 1. The images were obtained with V_{bias}= +1V (sample potential), I=1 nA, and a scan area of 1 nm^2. A model of the underlying atomic structure is shown as a guide to the eye. (a) Image from a single-layer of graphene (region I of Fig. 1). A honeycomb structure is observed. (b) Image of the multi-layer portion of the sample (region II of Fig 1). The characteristic "three-for-six" STM image of the surface of bulk graphite is observed.

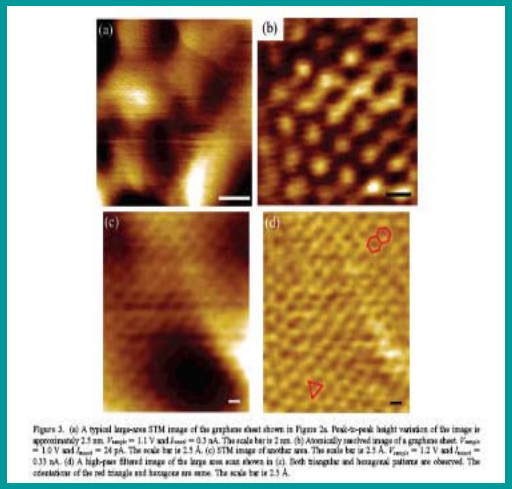

Figure 3. (a) A typical large-area STM image of the graphene sheet shown in Figure 2a. Peak-to-peak height variation of the image is approximately 2.5 nm. V_{sample} = 1.1 V and I_{tunnel} = 0.3 nA. The scale bar is 2 nm. (b) Atomically resolved image of a graphene sheet. V_{sample} = 1.0 V and I_{tunnel} = 24 pA. The scale bar is 2.5 Å. (c) STM image of another area. The scale bar is 2.5 Å. V_{sample} = 1.2 V and I_{tunnel} = 0.33 nA. (d) A high-pass filtered image of the large area scan shown in (c). Both triangular and hexagonal patterns are observed. The orientation of the red triangle and hexagons are same. The scale bar is 2.5 Å.

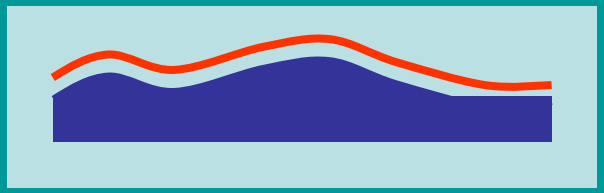

The graphene layer follows the corrugation of the substrate

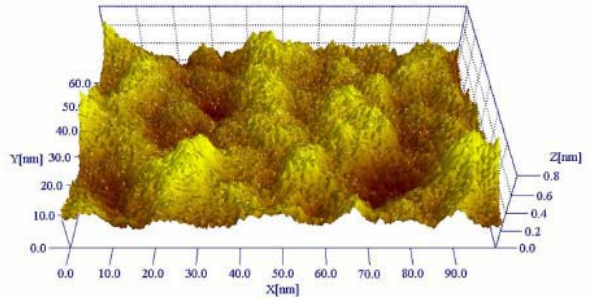

Figure 3. Stereographic plot of a large-scale (100×62 nm) STM image of a single-layer graphene film on the silicon dioxide surface. The STM scanning conditions were: V_{bias}= 1V (sample potential) and I=0.6 nA. The 0.8-nm scale of the vertical (Z) coordinate is greatly enlarged to accentuate the surface features.

Scattering by ripples

F. G. ArXiv:0805.3908, J. Low Temp. Phys., in press

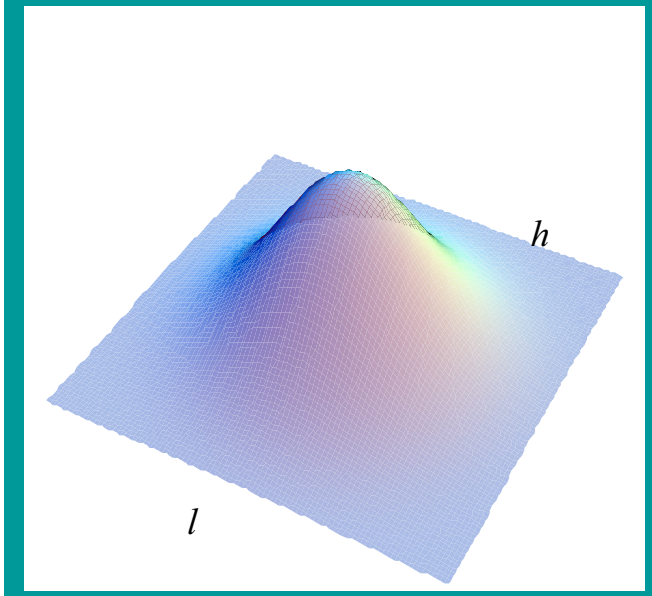

Born approximation

$$\sigma(\theta) \propto \{1+\cos[3(\theta_{out}+\theta_{in})]\} \times \begin{cases} \left(\frac{\partial \log(t)}{\partial \log(a)}\right)^2 \frac{k_F h^4 (k_F l)^4}{a^2} & k_F l \ll 1 \\ \left(\frac{\partial \log(t)}{\partial \log(a)}\right)^2 \frac{k_F h^4}{a^2} & k_F l \approx 1 \\ \left(\frac{\partial \log(t)}{\partial \log(a)}\right)^2 \frac{k_F h^4}{a^2 (k_F l)^4} & k_F l \gg 1 \end{cases}$$

- The cross section does not have a monotonous dependence on the carrier density.
- The angular dependence reflects the trigonal symmetry of the lattice.

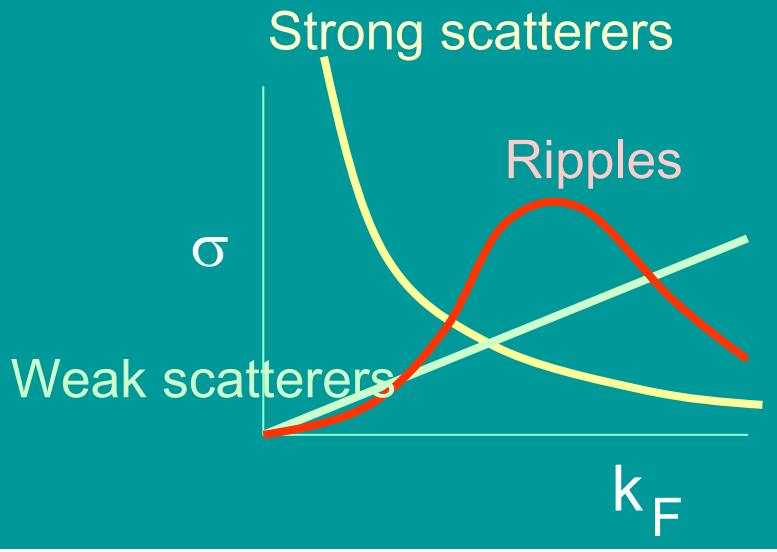

Model of the electronic structure of rippled graphene

F. G., M. I. Katsnelson, M. A. H. Vozmediano, Phys. Rev. B 77, 075422 (2008)

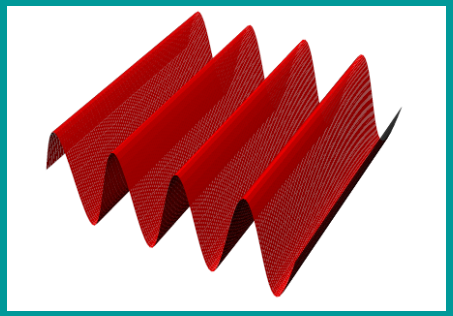

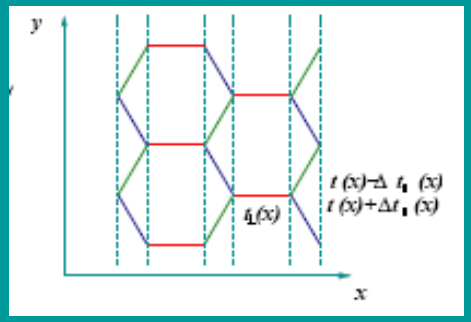

The ripples modulate the hoppings and change the electronic wavefunctions.

$$t \quad \leftrightarrow \quad t_{\parallel}(x)$$

$$2t\cos\left(\frac{k_y a\sqrt{3}}{2}\right) \quad \leftrightarrow \quad \sqrt{\bar{t}_{\perp}^2(x)\cos^2\left(\frac{k_y a\sqrt{3}}{2}\right)+\Delta t_{\perp}^2(x)\sin^2\left(\frac{k_y a\sqrt{3}}{2}\right)}$$

Modulation of the hoppings

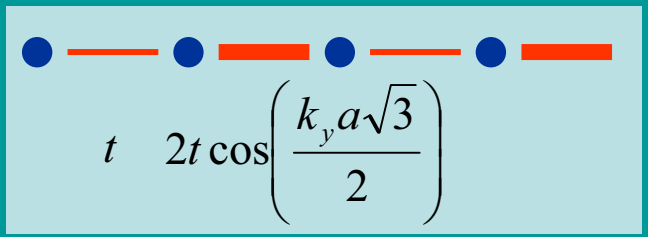

Effective 1D model with two hoppings

$$2t\cos\left(\frac{k_y a\sqrt{3}}{2}\right) \quad \leftrightarrow \quad 2t\cos\left(\frac{\left(k_y + A_y(x)\right)a\sqrt{3}}{2}\right)$$

Effect of a magnetic field

Results

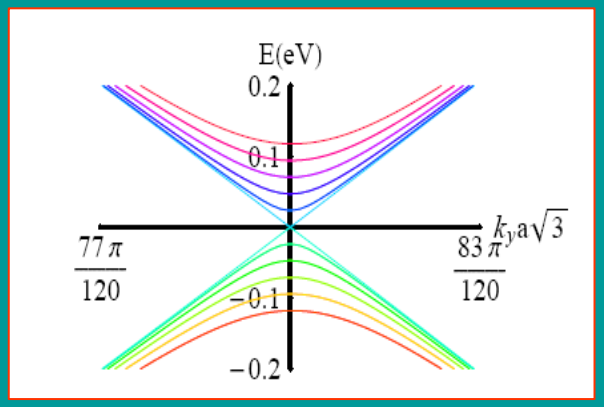

δt/t=0

There are well defined midgap levels

$$t_{\parallel}(x) = \delta t \sin\left(\frac{2\pi x}{l}\right)$$

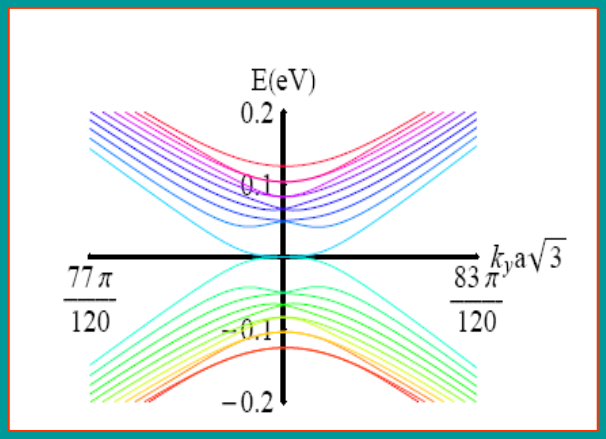

δt/t=0.02

The Dirac bands are recovered at high energies.

$$l_B \approx \sqrt{\frac{t}{\delta t}}\, la$$

$$\Delta \approx t\sqrt{\frac{\delta t}{t}\frac{a}{l}}$$

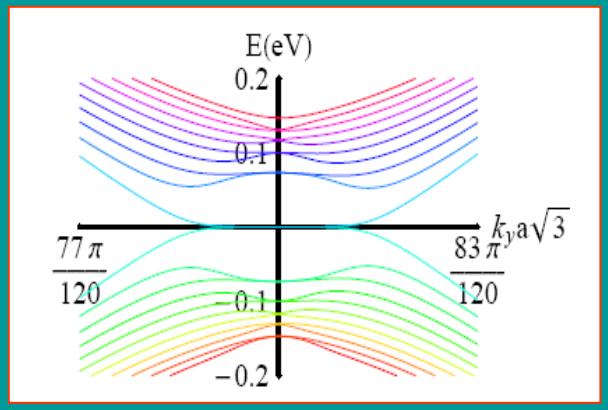

δt/t=0.04

l=1200a=168nm

Results. (Real) magnetic fields

B=10T, $\delta t/t=0.02$

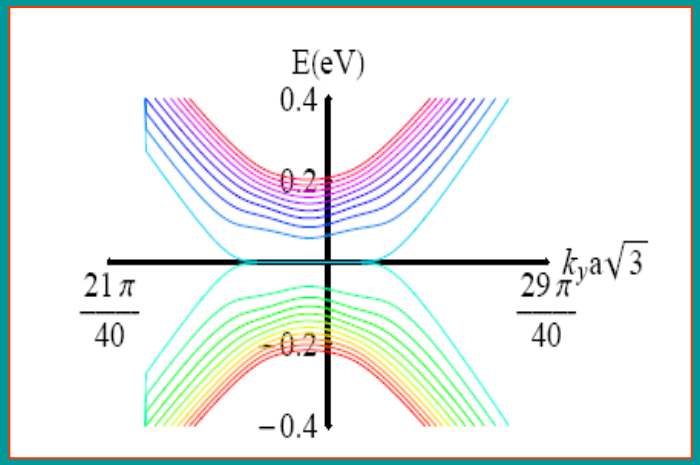

K point

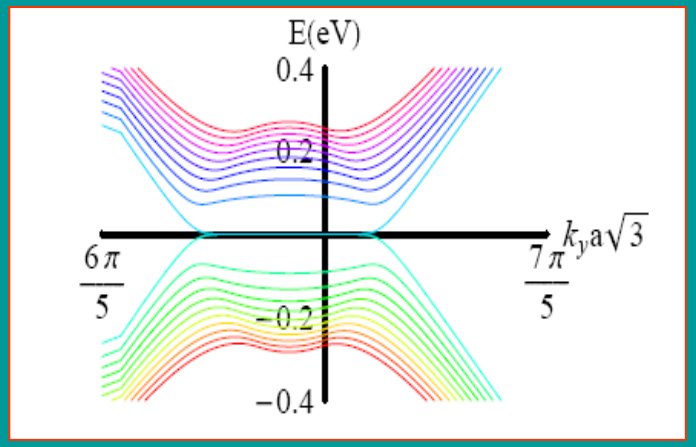

K' point

See also: E. Perfetto, J. González, F. G., S. Bellucci and P. Onorato, Phys. Rev. B **76**, 125430 (2006)

A real magnetic field breaks the symmetry between the two valleys: valleytronics.

A. Rycerz and J. Tworzydo and C. W. J. Beenakker, Nature Physics **3**, 172 (2007)

Electrons move around different cyclotron orbits, and are deflected differently by barriers.

V. V. Cheianov and V. I. Fal'ko, Phys. Rev. B **74**, 041403 (2006)

Effective flux through a ripple

F. G., M. I. Katsnelson and M. A. H. Vozmediano, Phys. Rev. B **77**, 075422 (2008)

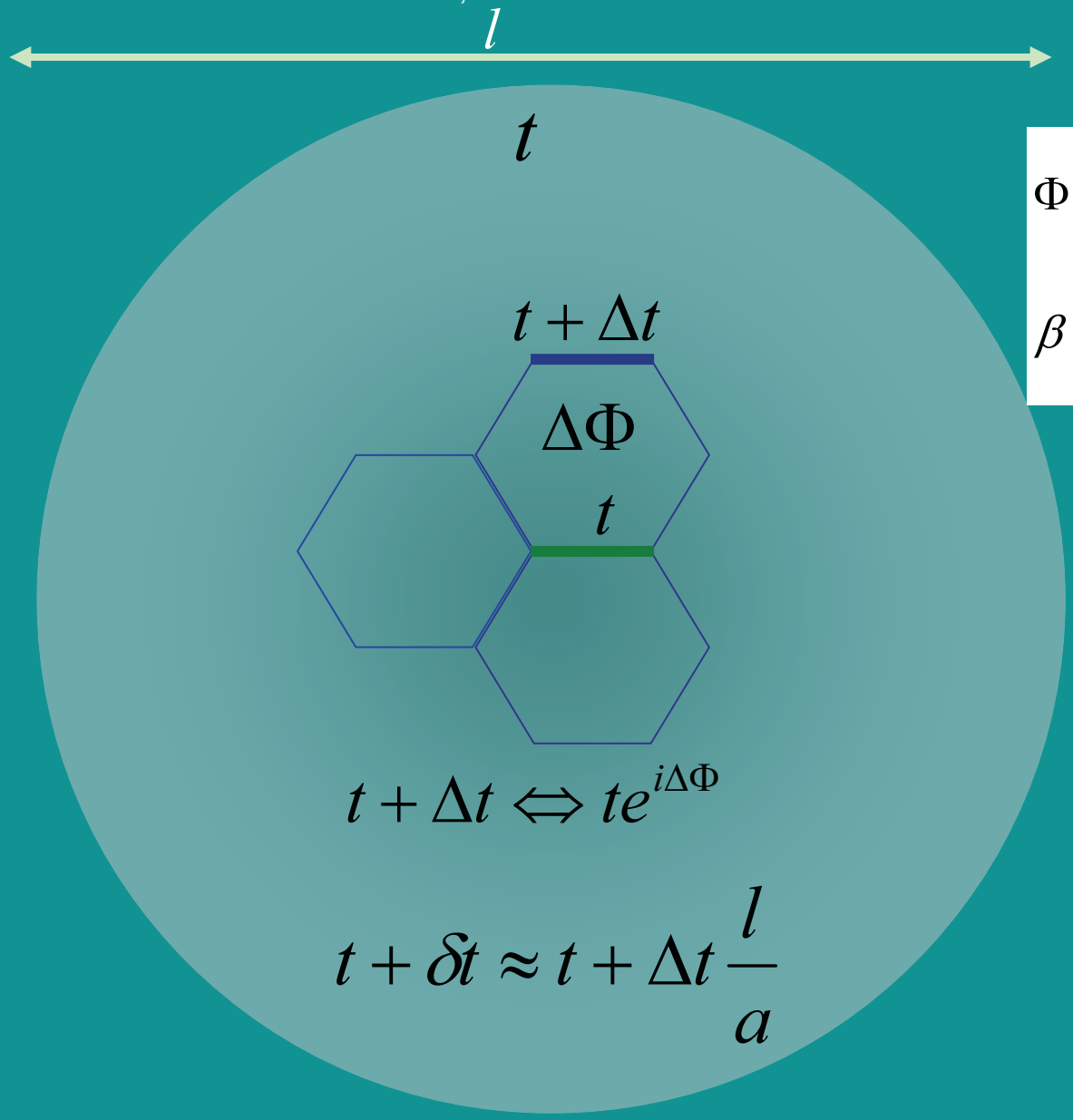

$$\Phi \approx \frac{\Delta t}{t}\frac{l^2}{a^2} \approx \frac{\delta t}{t}\frac{l}{a} \approx \frac{\partial \log(t)}{\partial \log(a)}\frac{h^2}{la}$$

$$\beta = \frac{\partial \log(t)}{\partial \log(a)} \approx 2$$

Φ is the number of Landau levels that fit into the ripple

The electronic wavefunctions are very different from Bloch states when $\Phi \geq 1$

Electron-electron interactions.

The electronic compressibility in clean graphene is zero. The electronic compressibility in graphene with ripples can be very large:

$$\kappa \approx \frac{e^{\Phi}}{\Delta l_B^2} \approx \frac{e^{\delta t l / t a}}{t a} \sqrt{\frac{\delta t}{t l a}}$$

The n=0 Landau level leads to many instabilities, see

M. O. Goerbig, R. Moessner and B. Doucot, Phys. Rev. B **74**, 161407 (2006)
K. Nomura and A. H. MacDonald, Phys. Rev. Lett. **96**, 256602 (2006)
H. A. Fertig and L. Brey, Phys. Rev. Lett. **97**, 116805 (2006)
J. Alicea and M. P. A. Fisher, Phys. Rev. B **74**, 075422 (2006)
V. P. Gusynin and V. A. Miransky and S. G. Sharapov and I. A. Shovkovy, Phys. Rev. B **74**, 195429 (2006)
V. A. Apalkov and T. Chakraborty, Phys. Rev. Lett. 97, 126801 (2006)
J.-N. Fuchs and P. Lederer, Phys. Rev. Lett. **98**, 016803 (2007)
D. A. Abanin, K. S. Novoselov, U. Zeitler, P. A. Lee, A. K. Geim and L. S. Levitov, Phys. Rev. Lett. **98**, 196806 (2007)
V. Lukose and R. Shankar, arXiv:0706.4280

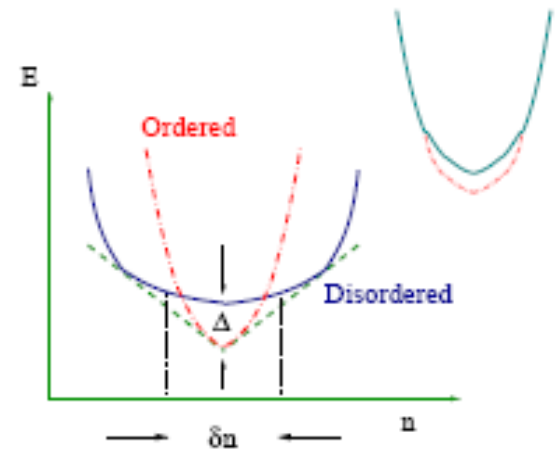

Electronic interactions will induce magnetic or charge ordering.
The high electronic compressibility favors a first order transition and electronic phase separation.

F. G., G. Gómez-Santos and D. P. Arovas, Phys. Rev. B **62**, 391 (2002)

An obvious possibility is a ferromagnetic state.

P. Esquinazi, D. Spemann, R. Höhne, A. Setzer, K.-H. Han and T. Butz, Phys. Rev. Lett. **91**, 227201 (2003)

Dirac electrons in a random gauge field

A. W. Ludwig, M. P. A. Fisher, R. Shankar, and G. Grinstein, Phys. Rev. B **50**, 7526 (1994)
B. Horovitz and P. Le Doussal, Phys. Rev. B **65**, 125323 (2002)
F. G., P. Le Doussal, B. Horovitz, Phys. Rev. B **77**, 205421 (2008)

Random gauge disorder.

$$\left\langle \vec{A}(\vec{r}), \vec{A}(\vec{r}') \right\rangle = \sigma \delta^{(2)}(\vec{r} - \vec{r}')$$

$$\left| \vec{r} - \vec{r}' \right| >> l$$

$$\rho(\varepsilon) \propto \varepsilon^{2/z-1}$$

$$z = \begin{cases} 2 - K + \sigma K^2 & \sigma < \dfrac{1}{2K^2} \\ K\left(\sqrt{8\sigma} - 1\right) & \sigma > \dfrac{1}{2K^2} \end{cases}$$

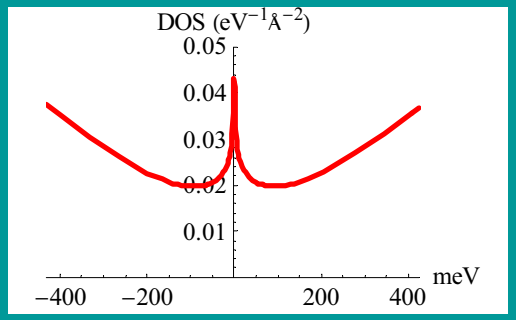

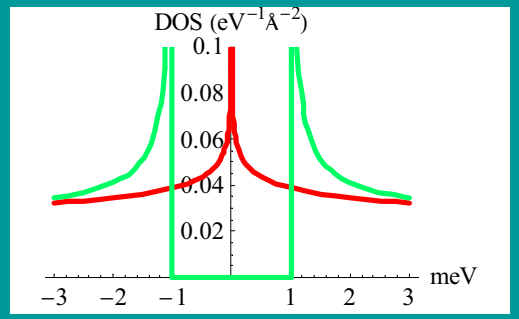

The density of states diverges for sufficiently large disorder.
Short range interactions become relevant.
A gap, Δ, can be induced

For ripples, the strength of the divergence is controlled by a dimensionless parameter:

$$\sigma \propto \beta^2 \frac{h^4}{l^2 a^2}$$

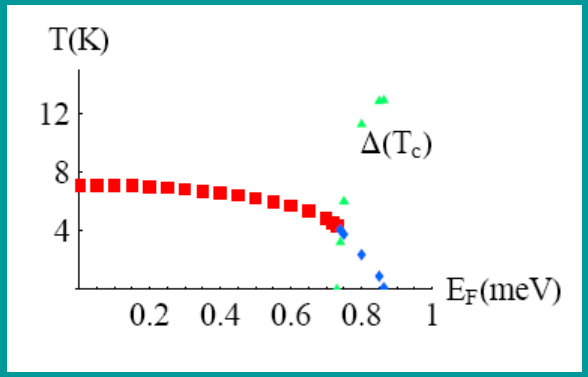

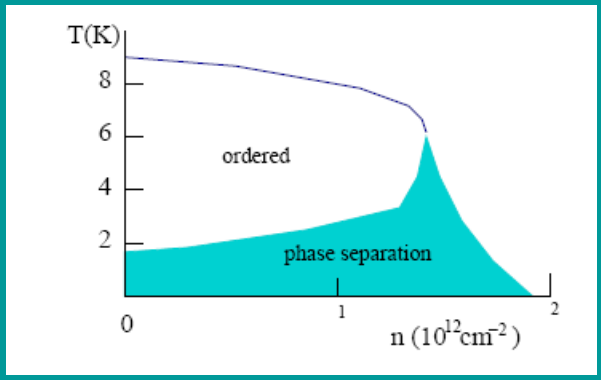

Ordered phase at low temperatures.
The transition is first order, leading to electronic phase separation

Midgap states and electronic instabilities. Models.

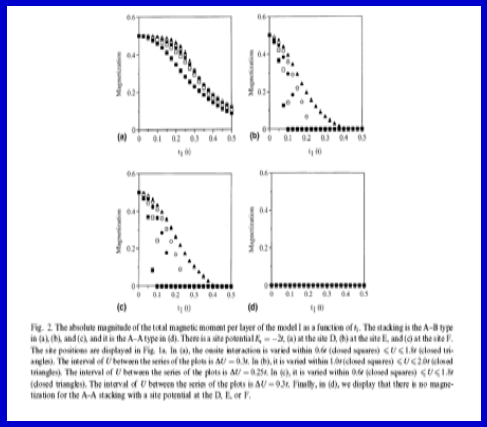

Fig. 2. The absolute magnitude of the total magnetic moment per layer of the model I as a function of t_1. The stacking is the A–B type in (a), (b), and (c), and it is the A–A type in (d). There is a site potential $E_s = -2t$, (a) at the site D, (b) at the site E, and (c) at the site F. The site positions are displayed in Fig. 1a. In (a), the onsite interaction is varied within $0.6t$ (closed squares) $< U \leq 1.8t$ (closed triangles). The interval of U between the series of the plots is $\Delta U = 0.3t$. In (b), it is varied within $1.0t$ (closed squares) $< U \leq 2.0t$ (closed triangles). The interval of U between the series of the plots is $\Delta U = 0.25t$. In (c), it is varied within $0.6t$ (closed squares) $< U \leq 1.8t$ (closed triangles). The interval of U between the series of the plots is $\Delta U = 0.3t$. Finally, in (d), we display that there is no magnetization for the A–A stacking with a site potential at the D, E, or F.

K. Harigaya and T. Enoki, Chem. Phys. Lett. **351**, 128 (2002)

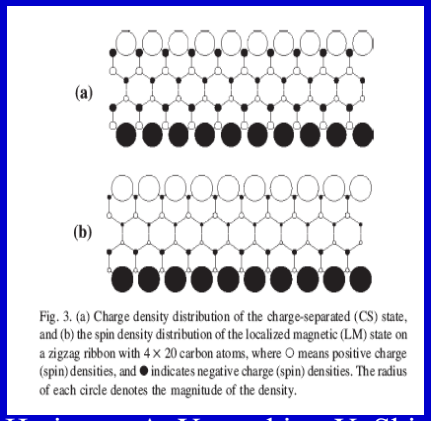

Fig. 3. (a) Charge density distribution of the charge-separated (CS) state, and (b) the spin density distribution of the localized magnetic (LM) state on a zigzag ribbon with 4 × 20 carbon atoms, where ○ means positive charge (spin) densities, and ● indicates negative charge (spin) densities. The radius of each circle denotes the magnitude of the density.

K. Harigaya, A. Yamashiro, Y. Shimoi, K. Wakayabashi, Y. Kobayashi, N. Kawatsu, K. Takai, H. Sato, J. Ravier, T. Enoki, M. Endo, Journ. Phys. Chem. Sol. **65**, 123 (2004)

Zigzag edges

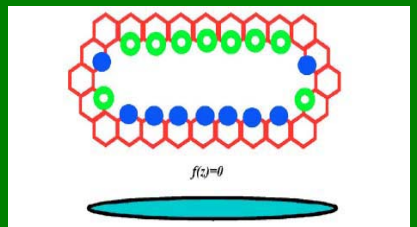

FIG. 1. (Color online) Elongated crack in the honeycomb structure. The crack is such that the sites in the upper edge belong to one sublattice, while those at the lower edge belong to the other. Bottom: an approximate cut in the complex plane that can be used to represent this crack at long distances.

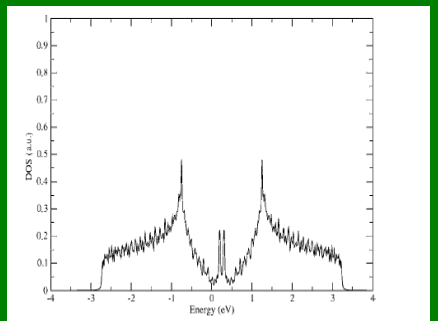

FIG. 4. The same as Fig. 3 with an on-site interaction $U=0.5t$.

M. A. H. Vozmediano, M. P. López Sancho, and F. G., Phys. Rev. B **72**, 155121 (2005)

Cracks, voids

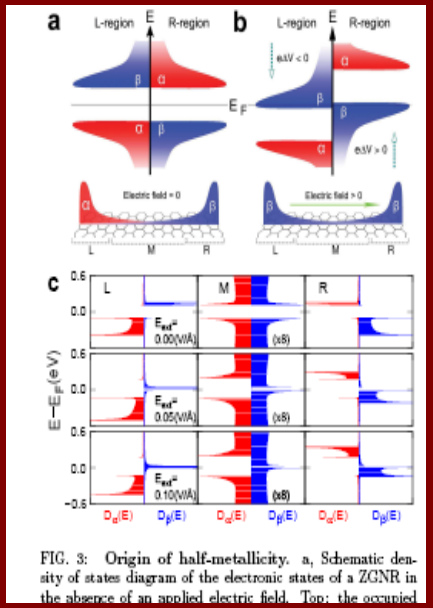

FIG. 3: Origin of half-metallicity. a, Schematic density of states diagram of the electronic states of a ZGNR in the absence of an applied electric field. Top: the occupied

Y.-W. Son, M. L. Cohen, and S. G. Louie, Nature **444**, 347 (2006)

Zigzag edges, revisited

Midgap states and electronic instabilities. Experiments.

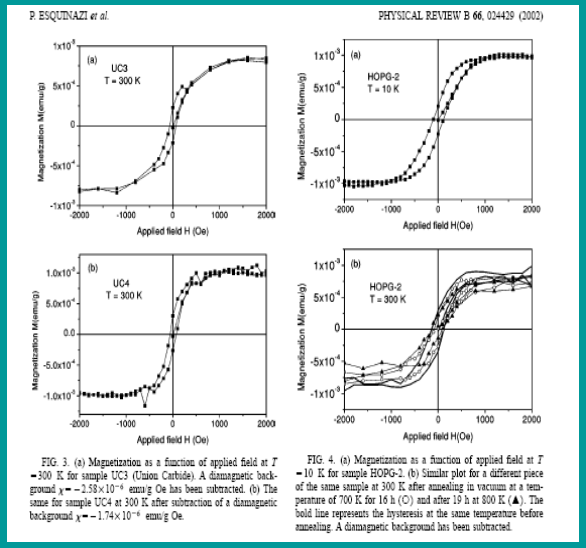

FIG. 3. (a) Magnetization as a function of applied field at $T = 300$ K for sample UC3 (Union Carbide). A diamagnetic background $\chi = -2.58\times10^{-6}$ emu/g Oe has been subtracted. (b) The same for sample UC4 at 300 K after subtraction of a diamagnetic background $\chi = -1.74\times10^{-6}$ emu/g Oe.

FIG. 4. (a) Magnetization as a function of applied field at $T = 10$ K for sample HOPG-2. (b) Similar plot for a different piece of the same sample at 300 K after annealing in vacuum at a temperature of 700 K for 16 h (○) and after 19 h at 800 K (▲). The bold line represents the hysteresis at the same temperature before annealing. A diamagnetic background has been subtracted.

P. Esquinazi, A. Setzer, C. Semmelhack, Y. Kopelevich, D. Spemann, T. Butz, B. Kohlstrunk, and M. Lösche, Phys. Rev. B **66**, 024429 (2002)

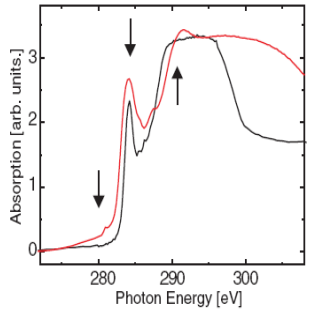

FIG. 2 (color). Carbon K-edge absorption spectrum (bottom) obtained from the sample prepared at room temperature (black) and at 560 °C substrate temperature (red). The arrows indicate the photon energies for which the STXM images (top) in the corresponding columns were acquired for a spot irradiated at 50 nC/μm^2 in sample A. The helicity (σ) of the x rays was reversed between the first and the second row of images. For the third row the direction (μ) of the applied field was reversed as well so that both polarization and applied field are opposite to the situation in the first row. Images acquired at the π^* resonance (284.0 eV) exhibit a clear XMCD signal.

H. Ohldag, T. Tyliszczak, R Höhne, D. Spemann, P. Esquinazi, M. Ungureanu, and T. Butz, Phys. Rev. Lett. **98**, 187204 (2007)

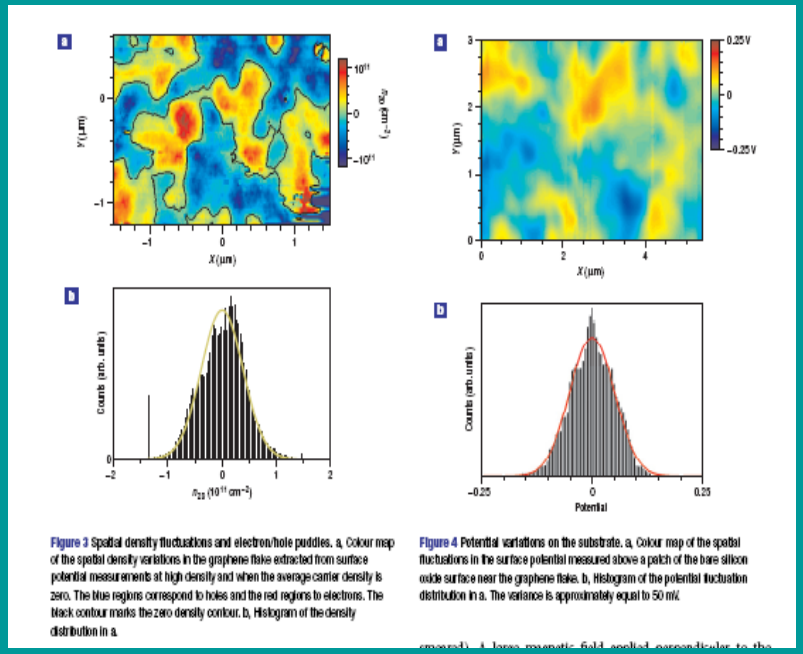

Figure 3 Spatial density fluctuations and electron/hole puddles. a, Colour map of the spatial density variations in the graphene flake extracted from surface potential measurements at high density and when the average carrier density is zero. The blue regions correspond to holes and the red regions to electrons. The black contour marks the zero density contour. b, Histogram of the density distribution in a.

Figure 4 Potential variations on the substrate. a, Colour map of the spatial fluctuations in the surface potential measured above a patch of the bare silicon oxide surface near the graphene flake. b, Histogram of the potential fluctuation distribution in a. The variance is approximately equal to 50 mV.

J. Martin, N. Akerman, G. Ulbricht, T. Lohmann, J. H. Smet, K. v. Klitzing, and A. Yacoby, Nature Phys. **4**, 144 (2008)

Electrostatic interactions and disorder.

T. Stauber, F. G. and M. A. H. Vozmediano, Phys. Rev. B **71**, 041406 (2005)
J. Ye, Phys. Rev. B **60**, 8290 (1999).
I. F. Herbut, V. Juricic, and O. Vafek, Phys. Rev. Lett. **100**, 046403 (2008)

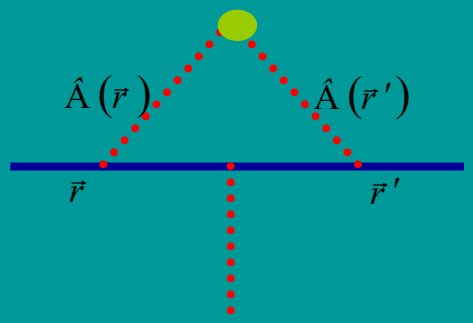

- There are selfenergy and vortex corrections.
- The selfenergy induces wavefunction renormalization.
- The vortex corrections depend on the type of disorder.
- The wavefunction renormalization changes the flow of the coupling constant.

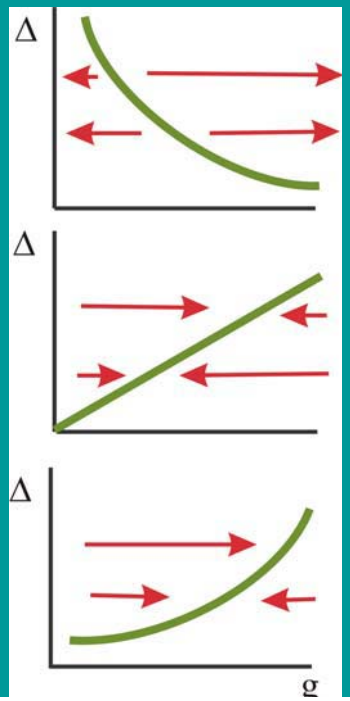

Smooth random potential

Coarse grained lattice defects

Smooth staggered potential

Ballistic transport in suspended graphene

M. M. Fogler, F. G., M. I. Katsnelson, ArXiv: 0807.3165

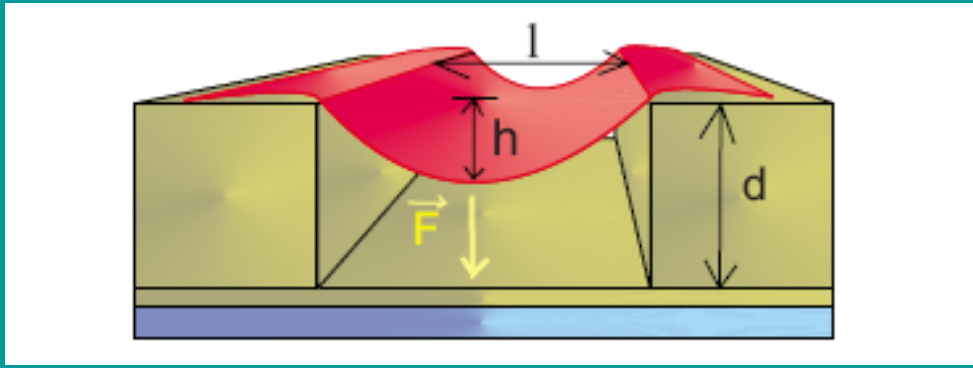

- The graphene layer is deformed by the applied electric field, slack, …
- Stresses lead to effective gauge potentials

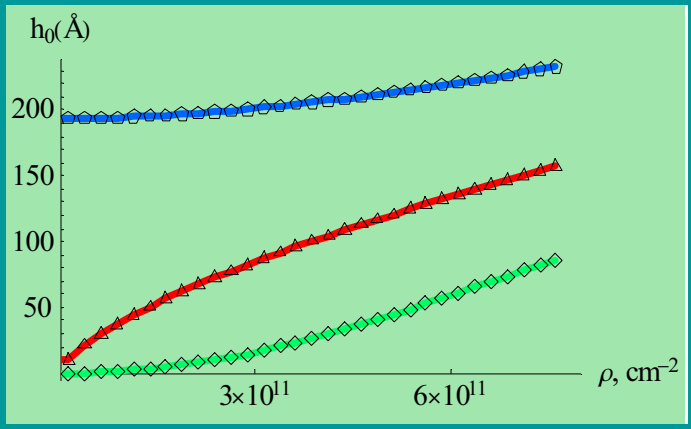

Maximum height as function of carrier density for different values of the slack

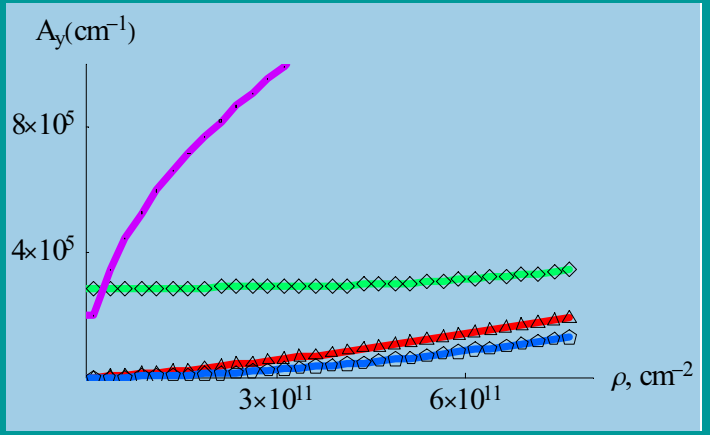

Vector potential inside the suspended region as function of carrier density for different values of the slack

Ballistic transport in suspended graphene

M. M. Fogler, F. G., M. I. Katsnelson, ArXiv: 0807.3165

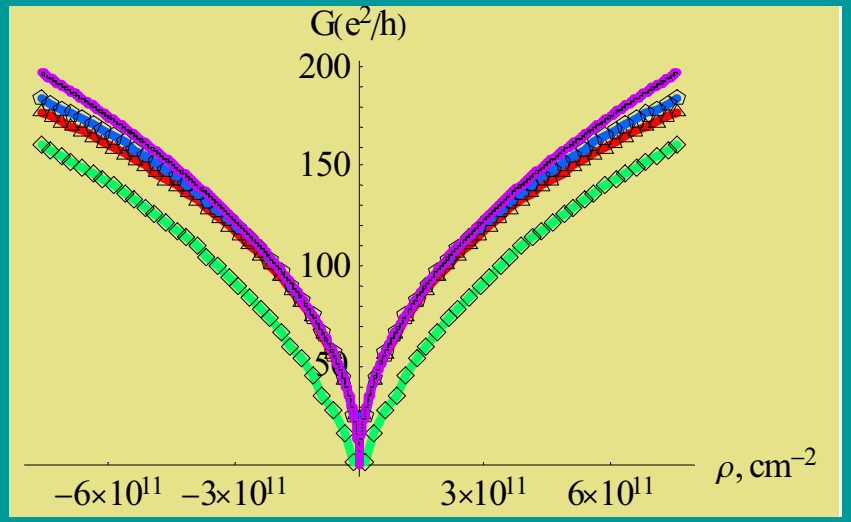

Transmission through a deformed graphene sheet as function of density for different values of the slack

Conclusions, open questions

- Fictitious gauge fields can be induced by strains, curvature, and topological defects
- Two non commuting gauge fields can be defined
- Height fluctuations can lead to significant fields.

$$\sigma = \frac{\partial \log(t)}{\partial \log(a)} \frac{h^2}{la} \approx 2 \frac{h^2}{la}$$

- Interaction effects may induce new phases at low carrier concentration.
- Strains and gauge fields will exist in suspended graphene samples under an applied field.
- Strains also induce scalar potentials,

S. Ono and K. Sugihara, Journ. Phys. Soc. Jap. **61**, 861 (1966)
H. Suzuura and T. Ando, Phys. Rev. B **65**, 235412 (2002)

- The orbits in a real magnetic field are modified.

Midgap states and charge instabilities in corrugated graphene, F. G., M. I. Katsnelson, and M. A. H. Vozmediano, Phys. Rev. B 77, 075422 (2008)

Gauge field induced by ripples in graphene, F. G., B. Horowitz and P. Le Doussal, Phys. Rev. B 77, 205421 (2008)

Pseudomagnetic fields and ballistic transport in suspended graphene sheets, M. M. Fogler, F. G., and M. I. Katsnelson, ArXiv:0807.3175

The electronic properties of graphene, A. H. Castro Neto, F. G., N. M. R. Peres,..A. K. Geim, K. S. Novoselov, ArXiv:0709.1163, Rev. Mod. Phys., in press